THE JOURNAL OF PHYSICAL CHEMISTRY B

Article

pubs.acs.org/JPCB

Mean-Square Displacement of Particles in Slightly Interconnected Polymer Networks

Erick Sarmiento-Gomez,[†] Iván Santamaría-Holek,[‡] and Rolando Castillo*,[†]

[†]Instituto de Física, Universidad Nacional Autónoma de México, P.O. Box 20-264, México, D.F. 01000, Mexico

[‡]UMDI Facultad de Ciencias, Universidad Nacional Autónoma de México, Campus Juriquilla, Querétaro 76230, México

ABSTRACT: Structural and viscoelastic properties of slightly interconnected polymer networks immersed in a solvent have been studied in two cases: when the polymer network is building up and when the polymer network is shrinking stepwise in a controlled way. To accomplish this goal, the mean square displacement (MSD) of embedded microspheres in the polymer network was measured as a function of time, with diffusive wave spectroscopy. Particle motion was analyzed in terms of a model, based on a Fokker–Planck type equation, developed for describing particles in Brownian motion within a network that constrain their movement. The model reproduces well the experimental features observed in the MSD vs t curves. The variation of the parameters describing the structure of the network can be understood as the polymerization comes about, and also after the successive volume contractions. In addition, from the MSD curves, the complex shear moduli were obtained in a wide range of frequencies when the network is building up, and at the different shrinking states of the network. Our microrheological results give an insight about the dynamics of embedded particles in slightly interconnected networks, which were also compared with similar results for polymers without interconnections and polymer gels.

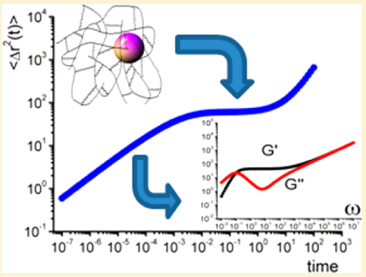

1. INTRODUCTION

Slightly interconnected polymer networks (IPNs) that are immersed in a liquid medium are materials forming a three-dimensional structure made of cross-linked entangled chains. Even though they are soft and structurally disordered and have a high volume fraction of liquid solvent, some of their mechanical properties are solid-like. A physical realization of this type of systems is the cross-linked polyacrylamide consisting of long linear flexible segments joined at a few cross-link points. It is formed by free-radical polymerization of acrylamide monomers and a small quantity of methylene bisacrylamide working as a cross-linker between polyacrylamide molecules. In general, when the cross-linker concentration is large enough, the acrylamide–bisacrylamide system forms a typical gel that in the last two decades has attracted much attention because of its scientific interest. Some examples can be mentioned such as the role of ionization of the polymer network in the phase swelling–shrinking transitions of this gel,[1,2] the formation of blob clusters and holes in swelling gels,[3] the friction coefficient between the polymer network gel and water,[4] the influence of cross-linkers and polymerization temperature on the polymerization process,[5] measurement of viscoelastic properties using dynamic light scattering, diffusing wave spectroscopy, and video-based particle tracking techniques,[6] identification of the gel point, and the critical scaling exponents using particle tracking microrheolgy.[7,8] The technological importance of these gels in biochemistry and molecular biology is nowadays outstanding.[9] In particular, when the number of cross-links is small, the slightly IPNs resemble biological scaffolds and they might be useful as model systems; however, the study of their viscoelastic properties has received much less attention.

If a small portion of acrylamide groups in the polymer network is hydrolyzed into ionizable acrylic acid groups, the polymer network can undergo continuous or discrete transitions of its equilibrium volume. This occurs when the polymer network is immersed in an acetone–water solution, and the solution composition or its temperature is varied.[1] This makes this soft material an excellent candidate to study how particle fluctuations evolve in a complex network as the volume of an interconnected polymer networks shrinks. The volume transition modifies the polymer network structure, and it has an important effect on one of the most important properties to be measured in rheology, the shear modulus, G, which connects stress response to an applied deformation in a material, $\sigma = \int_{-\infty}^{t} dt'\, G(t-t')\dot{\gamma}$; σ is the shear stress, and $\dot{\gamma}$ is the shear rate. The shear modulus exhibits a significant time, or frequency, dependence expressed through the complex modulus $G^*(\omega) = G'(\omega) + iG''(\omega)$. The real part of the complex modulus is the storage, or elastic, modulus in phase with the applied shear strain. The imaginary part is the viscous, or loss, modulus in phase with $\dot{\gamma}$.

Viscoelastic properties are usually measured with mechanical rotational rheometers that probe macroscopic samples in a limited frequency range ($\omega \sim 10^{-2}$ to 30 rad/s), and in various deformation geometries; their use depends on the extent of strain and the magnitude of shear modulus to be measured.

Received: October 24, 2013
Revised: January 14, 2014
Published: January 14, 2014

dx.doi.org/10.1021/jp4105344 | J. Phys. Chem. B 2014, 118, 1146–1158

However, when the rheology of a polymer network is assessed, these mechanical rheometers may destroy or substantially affect the internal structure, leading to nonaccurate results. Other kinds of mechanical rheometers have been developed for reaching high frequencies (>10 kHz) and applying very low strain amplitudes, as those using piezo-driven oscillatory devises or torsional resonators.[17]

Microrheological techniques are another option for measuring viscoelastic properties. They have been reliable to get useful structural and dynamic information in soft materials,[14−20] because the modification of the measured material is avoided or reduced to a minimum. The general principles behind microrheology are two: first, minimization of the mechanical probe that deforms matter, typically, a colloidal particle in random motion; second, employment of a modern technique for tracing the probe particle motion (optical microscopy, light scattering, etc.). A colloidal particle is a delicate probe, which introduces a minimum perturbation in the structure and dynamics of fragile soft matter (thermal energies $\sim k_B T$; k_B is the Boltzmann's constant and T is the temperature), allowing the measurement of rheological properties at the micrometer and submicrometer scales through evaluating the mean square displacement (MSD = $\langle \Delta\boldsymbol{\rho}^2(t) \rangle$) of particles. In microrheology, $G^*(\omega)$ can be evaluated from the MSD in a wide range of frequencies, making this procedure a good option when the limitations of standard mechanical rheology are an issue, for instance, the range of frequencies, the size of the shear moduli that can be probed, the sample size, and the fragility or heterogeneity of specimen to be measured.

Movement of embedded particles within IPNs is just determined by the interaction of particles with the solvent and the polymer molecules, if they are dilute. The relevant factors for particle motion are particle size, concentration of the polymer, geometrical arrangement of the polymer chains, and the stiffness of the chains. The theoretical description of these factors can be carried out by means of several approaches, although the most important contribution to particle diffusion in a IPN comes from steric hindrance.[10,11] This steric hindrance is usually modeled in terms of an obstruction effect, which leads to a lengthening of the diffusion path that has been investigated with computer simulations.[12,13] Brownian motion of particles in polymer networks can be experimentally studied through measuring their MSD as a function of time, by means of the mentioned microrhelogical techniques, which help to understand the mechanisms that lead to subdiffusive dynamics. Here, diffusion does not scale linearly with time, an issue that remains unsolved when the host material displays a variety of time and length scales, as in the case of particles embedded in IPNs. Several effects emerge in anomalous diffusion: a broad distribution of jump times, a broad distribution of jump lengths, or strong correlations in diffusive motion. Particularly, obstruction and caging occurring in IPNs produce strong correlations, because the local isotropy of space breaks down.

For highly cross-linked polyacrylamide, dynamic viscoelastic spectra have been measured in real time during gelation, at small strains, placing the gel directly between the parallel rheometer plates.[21] A linear increase of $G'(\omega)$, which is almost frequency independent, up to a maximal value was found when the mesh size was changed by modulating the molar ratio of the monomer and the cross-linker. It was also observed that $G'(\omega) \gg G''(\omega)$ and that $G'(\omega)$ increases linearly with T. A comparison among rheological moduli for cross-linked polyacrylamide−bisacrylamide, in the sol and the gel regimes, was made by Dasgupta and Weitz[6] employing polystyrene beads of several sizes and surface chemistry. They used data from bulk rheology, quasielastic light scattering, diffusing wave spectroscopy (DWS), and one-particle and two-particle microrheology. These authors could probe almost eight decades in frequency, which was not possible using traditional bulk rheometric measurements, validating the ability of microrheology for studying cross-linked polymeric systems. On the other hand, multiple tracking microrheolgy was successfully used to extract the full spectrum of rheological information near the gel point, including the critical extent of reaction by identification of the gel point, the critical relaxation exponent, and other critical dynamic scaling exponents.[7,8] Translation and rotational dynamics of optically anisotropic colloidal particles have been studied with depolarized light scattering, allowing us to calculate the translational and rotational MSD of particles embedded in highly cross-linked polyacrylamide gels.[22,23]

The purpose of this paper is to study the structural and viscoelastic properties of slightly IPNs immersed in a solvent in two cases: first, when the polymer network is building up, i.e., when the polymerization is taking place, and second, when a swollen polymer network is shrunk stepwise in a controlled way. To accomplish this goal, the MSD as a function of time is measured for microspheres embedded in the polymer networks. An optical technique, DWS, was used to follow the time evolution of the MSD of the microspheres. These experiments give structural and dynamic information about the network when used in conjunction with a model based on a Fokker−Planck equation. This model was explicitly developed to understand particle motion in a polymeric network that constrains the particle movement. The model is able to reproduce the experimental features observed in the MSD vs t curves. It allowed us to understand how the parameters characterizing the structure of the network change as the polymerization comes about, and when volume undergoes successive contractions. For the different studied circumstances, $G^*(\omega)$ was also calculated for a wide range of frequencies from the MSD curves. Our microrheological results for the slightly IPNs were compared with those obtained for polymer without cross-links, and for highly cross-linked polymeric gels previously reported in the literature. This article is organized as follows: In section 2, experimental procedures, techniques, and the experimental setup are described. Section 3 is presents a theoretical model developed for understanding the MSD experimental results. In section 4, we give our results, as well as a discussion. Finally, in section 5 we present the conclusions.

2. EXPERIMENTAL SECTION

2.1. Materials and Methods. The linear constituent acrylamide (prop-2-enamide ≥99.5%; Fluka), the cross-linking constituent bis-acrylamide (*N*,*N*′-methylene-bisacrylamide ≥99.5%; Fluka), the initiator APS (ammonium persulfate, 98%; Fluka), and the accelerator TEMED (*N*,*N*,*N*,*N*-tetramethylethylene diamine, 99%; Sigma-Aldrich) were used as received. Polystyrene probe microspheres with diameters 600 and 800 nm (Bangs Laboratories Inc., Fishers, IN, USA) and deionized water (Nanopure-UV; 18.3 MΩ cm) were used during all the experiments.

2.2. Polymer Samples. In all experiments microspheres were added and blended with weighted quantities of acrylamide (w_A), bisacrylamide monomers (w_B), and water (w_{H_2O}). Results are presented in total polymer concentration, %P = [(w_A +

dx.doi.org/10.1021/jp4105344 | J. Phys. Chem. B 2014, 118, 1146−1158

$w_B)/(w_A + w_B + w_{H_2O})] \times 100$, and in the cross-linker concentration, $\%C = [w_B/(w_A + w_B)] \times 100$. Therefore, the cross-linker concentration with respect to the total weight is $\%T = [w_B/(w_A + w_B + w_{H_2O})] \times 100 = \%P \times \%C/100$.

The transport mean free path, l^*, was also measured prior and after the polymerization, without any significant change. The ratios L/l^* were always between 12 and 20, to ensure the diffusive approximation of light transport in the sample without a significant light absorption; here, L is the sample size.

2.3. Experiments of Hydrolysis and Shrinking. After mixing the polymers and microspheres, the initiator (TEMED, 3.2 μL/ml) and the catalyst (5 μL/mL of a 10 wt % APS aqueous solution) were added to start the polymerization reaction in a cylindrical recipient, of height L, made of Teflon within a nitrogen atmosphere. The cross-linker concentration was very low, consequently, the polymerized polymer network did not scatter light (%C = 0.5, 1.0, 2.0); 0.13% of the total sample weight was the higher cross-linker concentration used. To hydrolyze a portion of the acrylamide groups ($-CONH_2 \rightarrow -COOH$), the polymerized samples were allowed to reach equilibrium with a basic solution of TEMED aqueous solution (0.4 vol %). After hydrolysis, the IPNs were equilibrated within acetone−water mixtures for 72 h. Prior to the DWS experiments, the l^* of the swollen IPNs was estimated by measuring the volume of the IPNs to get an approximate value of the swelling ratio, as well as of the particle volume fraction. DWS experiments were performed in a temperature-controlled cell filled with the corresponding acetone−water mixture to maintain the swollen IPN in thermal equilibrium.

2.4. Experiments for Following Polymerization. Mixtures of weighted quantities of acrylamide, bisacrylamide, water, and microspheres (diam = 800 nm, $\varphi = 0.0125$) were placed in DWS cells of thickness L, with a very slow nitrogen flow to avoid atmospheric oxygen interference during the polymerization process. After small quantities of initiator (1 μL) and catalyst (0.5 μL of our stock solution) were added to the mixture to start the polymerization reaction; small quantities of TEMED and APS produce very slow polymerization reactions. Typical polymerization times were in the range of 80 min; this was a convenient time interval because each DWS measurement lasted typically 2−3 min. The measurement time was a good compromise, with enough delay time to get a smooth intensity time correlation function, but shortly enough to observe a quasi-stationary state during such a slow the reaction process.

2.5. Diffusive Wave Spectroscopy (DWS). Our DWS setup is a homemade instrument described elsewhere.[43] DWS theory connects temporal field fluctuations of the scattered light emerging from a turbid suspension to the dynamics of the probe particles embedded in the suspension. $\langle \Delta\boldsymbol{\rho}^2(t)\rangle$ of the probe particles can be determined by collecting the scattered intensity from a single speckle over a sufficiently long collection period, and by evaluating the time-averaged intensity autocorrelation function (ACF), $g^{(2)}(\tau)$. The time-averaged field ACF, $g^{(1)}(\tau) = \langle E(0)\, E^*(t)\rangle/\langle |E(0)|^2\rangle$, is related to the measured $g^{(2)}(\tau)$ through the Siegert relation: $|g^{(2)}(\tau)| = 1 + \beta|g^{(1)}(\tau)|^2$, where β is an instrumental factor determined by the collection optics. Therefore, the Brownian motion of probe particles incorporated in the fluid of interest is tracked with multiple dynamic light scattering experiments, when laser light is incident on one side of a planar sample and the scattered light is collected from a small area on the opposite side. A single photon passing through the sample undergoes n scattering events and emerges with a phase that depends on its total path length; photons are multiply scattered and lose their scattering vector dependence. The total phase shift of the photon after passing from the laser to the detector can be calculated, and the total field at the detector is the superposition of the fields from all light paths through the sample to the detector. Therefore, the temporal electric field fluctuations of the scattered light emerging from the suspension can be connected to the motion of the particles incorporated in the fluid. In a transmission geometry, the polymer network under investigation with the scattering particles immersed in it, can be treated as a slab with an infinite transverse extent and a thickness $L \gg l^*$. After traveling a l^* distance, light propagation is randomized and the transport of light in a turbid medium can be described by the diffusion approximation.[24−27] In this case, the expression of the time-averaged field ACF, $g^{(1)}(\tau)$ is[24−27]

$$g^{(1)}(t) = \frac{\frac{L/l^*+4/3}{\alpha^*+2/3}\left(\sinh[a^*x] + \frac{2}{3}x\cosh[a^*x]\right)}{\left(1 + \frac{4}{9}x^2\right)\sinh\left[\frac{L}{l^*}x\right] + \frac{4}{3}x\cosh\left[\frac{L}{l^*}x\right]} \quad (1)$$

where $x = [Q_0^2\langle \Delta\boldsymbol{\rho}^2(t)\rangle]^{1/2}$, $\alpha^* = z_0/l^*$, and z_0 is the distance into the sample from the incident surface to the place where the diffuse source is located. $Q_0 = 2\pi n_s/\Lambda$ is the photon wave vector in the solvent, Λ is the light wavelength in vacuum, and n_s is the index of refraction in the solvent. If l^* is known for a sample with embedded particles, the MSD of a probe particle can be obtained by using eq 1.

The ability to store energy upon deformation changes the temporal correlations of the stochastic forces acting on the particle at thermal equilibrium, because the suspending medium must satisfy the fluctuation−dissipation theorem. In microrheology, it is assumed[27−30] that the material time-dependent memory function, $\zeta(t)$, which accounts for both the energy loss and storage upon deformation, is proportional to the bulk-frequency dependent viscosity of the fluid, $\tilde{\eta}(s) = \tilde{\zeta}(s)/6\pi a$. The relation between $\tilde{G}(s)$ and $\langle \Delta\boldsymbol{\rho}^2(t)\rangle$ can be written as[29]

$$\tilde{G}(s) = s\tilde{\eta}(s) = \frac{s}{6\pi a}\left[\frac{6k_BT}{s^2\langle \Delta\tilde{\rho}^2(s)\rangle} - ms\right] \quad (2)$$

Here, s is the frequency in the Laplace domain, and m and a are the mass and the radius of the particle, respectively. Using the unilateral Fourier transform F_u, and neglecting the inertial term, an expression for the viscoelastic modulus as a function of frequency can be written as[29]

$$G^*(\omega) = G'(\omega) + iG''(\omega) = \frac{k_BT}{\pi a i\omega F_u[\langle \Delta\rho^2(t)\rangle](\omega)} \quad (3)$$

Several procedures have been followed by different authors[29−33] to determine F_u. In our case, the logarithmic derivative of the MSD was evaluated on experimental data fitted curves. The viscoelastic modulus were calculated using eq 3.[29]

2.6. Two-Cell Technique and Multispeckle DWS. Time-averaged ($\langle ... \rangle_T$) and ensemble-averaged ($\langle ... \rangle_E$) correlation functions are identical, when all the scattering particles suspended in a fluid are free to explore the same local environment during the course of a measurement; the scattering process is ergodic. If particles are bounded near a fixed position or if they are arrested, time averaging and ensemble averaging are not equivalent. To overcome this

situation, Scheffold et al.[34] proposed a method for obtaining true-ensemble average autocorrelation functions. Here, light transmitted through a sandwich of two turbid cells then can be considered as ergodic even though only one of the cells is ergodic. The use of a second cell modifies the intensity correlation function of transmitted light, which now exhibits an additional decay. To simplify the analysis of the experimental data, the parameters of the double-cell sample can be optimized. Namely, moderate absorption and/or leakage of light should be introduced between the two cells, and the optical thickness of the ergodic cell should be reduced well below the optical thickness of the cell containing the nonergodic medium; at the same time, the dynamics of scatterers in the ergodic cell should be chosen to be slow. Under these conditions, Scheffold et al.[34,35] have shown that the field autocorrelation function of light transmitted through the double-layer sample can be written as a multiplication rule. The two-cell geometry can also be realized using a very slowly rotating diffuser disk, as suggested by Viasnoff et al.[36] This method provides a procedure for obtaining accurate autocorrelation functions in turbid, nonergodic media in time scales below the characteristic decorrelation time of the second ergodic cell. In our case, we used a rotating diffuser disk made of ground glass connected to a slow-working motor. The decay correlation time was found to lie around the 20 ms. For slow dynamics, we used a CCD camera as a light detector. With this approach it is possible to record simultaneously a large number of speckles, and thereby to obtain direct multispeckle ensemble-averaged autocorrelation functions. The autocorrelation function at a lag time is calculated by an algorithm that compares the speckle field image at a time delay from fixed reference time. The speckle size was adjusted to obtain a satisfactory optical contrast with as many speckles as it was possible to be analyzed.[37] The frame rate of the camera is around 100 frames/s, allowing detection of the autocorrelation function at delay times as small as 10 ms. Our set up is described in ref 43.

2.7. Intensity Correlation Functions for the Case of Nonergodic Systems. In Figure 1, we present the normalized intensity correlation functions of interest vs time delay obtained with DWS and with multispeckle DWS. For relative short lag times ($\tau \leq 10$ ms) the multiplication rule for intensity correlation functions was used.[34,35] Here, the scattered light of the sample was mixed with the light scattered from a slow rotating disk into a photomultiplier detector.[34−36] Under the current configuration of our DWS setup, the multiplication rule holds, i.e., $g_2^M(t) = g_2^E(t) \times g_2^S(t)$ where M, E, and S correspond to the mixed signal, the ergodic sample, and the sample under study, respectively. Thereby, by knowing the intensity autocorrelation functions coming from the rotating diffusing disk and the mixed one, the ensemble-averaged autocorrelation function of the sample can be retrieved. Figure 1 shows the rotating diffusing disk autocorrelation function (red line), $g_2^E(t)$, the mixed signal (black line), $g_2^M(t)$, and the retrieved ensemble-averaged sample signal (black filled circles), $g_2^S(t)$. As indicated by the multiplication rule, this method provides a procedure for obtaining ensemble-averaged autocorrelation functions at times scales below the characteristic decorrelation time of the rotating diffusing disk (~10 ms). Figure 1 also shows the autocorrelation function obtained by multispeckle DWS obtaining with a CCD device. The red filled circles represent the raw autocorrelation function that has to be corrected. First, by subtracting the artificial baseline and then by adjusting (normalizing) the height of the correlation function with the correlation function obtained using the rotating diffusing disk. This produces the hollow black circles that in conjunction with the filled black circles provide the full ensemble-averaged autocorrelation function ranging through 9 decades in time.

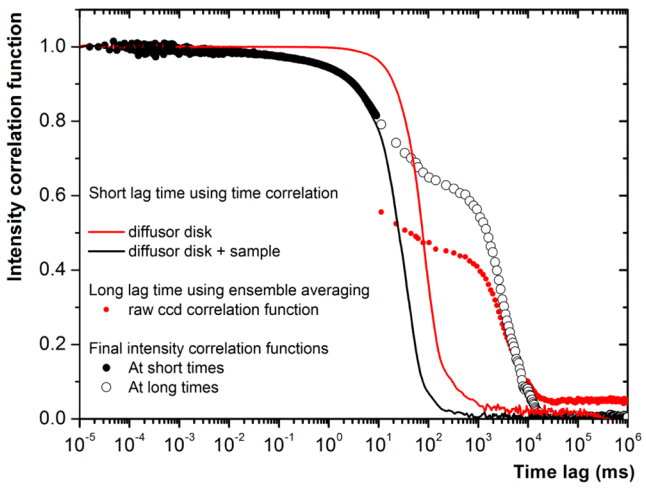

Figure 1. Intensity correlation functions obtained with DWS and with multispeckle DWS (see text). The final intensity correlation function of the sample is the curve formed by filled and hollow black circles.

3. THEORETICAL MODEL FOR CONSTRAINED DIFFUSION

The motion of submicrometer particles in an IPN can be analyzed by considering that each particle performs a partially constrained diffusion within polymeric cages or cells. Our model starts by assuming that the dynamical state of each particle in the network can be determined by means of two configuration variables. One characterizing the position $\mathbf{R}_i$ of the geometrical center of the fluctuating cell formed by the polymer network, where the position of the particle is fluctuating. A second one determines the position $\mathbf{r}_i$ of the fluctuating particle with respect to the center of the cell. The position of the particle with respect to a lab-coordinate axis, $\boldsymbol{\rho}_i$, is given as the sum of both position vectors, $\boldsymbol{\rho}_i = \mathbf{R}_i + \mathbf{r}_i$. This description allows a better understanding of the effects of confinement, and the activated process related to the escape of particles from one cell to other.

The characteristic scales of the motion will be $r_i \leq \lambda$ and $R_i \geq \lambda$. Here, λ represents a characteristic length of the polymeric cells, mainly determined by bisacrylamide filaments joined to acrylamide filaments at cross-link points. Therefore, λ can be related to the characteristic length of the network (mesh size). Two characteristic time scales can be introduced, one related to particle diffusion inside each cell $\tau_r = a^2/D_0$ with a the radius of the particle and D_0 the short-time diffusion coefficient, which is assumed to be given by the Stokes−Einstein relation, $D_0 = k_B T \beta_0$; β_0 is a short-time mobility, i.e., the inverse Stokes friction coefficient, which turns out to be proportional to the local viscosity η_0 of the host fluid. The other time scale, associated to R, is $\tau_R = \lambda^2/D_R$ with $D_R = k_B T \xi_0$ and ξ_0 is a long-time mobility.

We start our description in terms of a normalized single-particle time dependent distribution function, $f(\mathbf{r},\mathbf{R},t)$, that satisfies a continuity equation of the form[38]

dx.doi.org/10.1021/jp4105344 | J. Phys. Chem. B 2014, 118, 1146−1158

$$\frac{\partial f(\mathbf{r},\mathbf{R},t)}{\partial t} = -\frac{\partial}{\partial \mathbf{r}}\cdot(\mathbf{v}_r f) - \frac{\partial}{\partial \mathbf{R}}\cdot(\mathbf{V}_R f) \tag{4}$$

where $\mathbf{v}_r f$ and $\mathbf{V}_R f$ are the associated probability currents in the ($\mathbf{r}$, $\mathbf{R}$) space. These two quantities can be determined by analyzing the entropy produced by an ensemble of particles during the diffusion process, and then by following the rules of nonequilibrium thermodynamics.[39] The entropy production can be calculated considering the Gibbs entropy postulate:[38,40]

$$S(t) = S_{leq} - k_B \int f \ln\left|\frac{f}{f_{leq}}\right| d\mathbf{r}\, d\mathbf{R} \tag{5}$$

where the local equilibrium distribution function $f_{leq}(\mathbf{r},\mathbf{R})$ is given by the Boltzmann factor

$$f_{leq}(\mathbf{r},\mathbf{R}) = Z^{-1}(T)\exp\left[-\frac{U(\mathbf{r},\mathbf{R})}{k_B T}\right] \tag{6}$$

Here, $Z(T)$ is the partition function; $U(\mathbf{r},\mathbf{R})$ is the potential energy of the particles that can be divided into a local $U_r(\mathbf{r})$ and an intercage $U_R(\mathbf{R})$ contributions, $U(\mathbf{r},\mathbf{R}) = U_r + U_R$. In general, the confinement of a particle in a cell may depend on the position of the cell in the system. Therefore, it is a function of $\mathbf{R}$ and its fluctuations, characterized by $\langle \mathbf{R}^2\rangle$. If we assume, in a first approximation, that the interaction of a particle with the elements of the network is elastic, we may write the local contribution to the energy, U_r, in the form

$$U_r(\mathbf{r},\mathbf{R}) = \frac{1}{2}k_R(\mathbf{R})\mathbf{r}^2 \tag{7}$$

where $k_R(\mathbf{R})$ is an $\mathbf{R}$-dependent elastic constant that takes into account the heterogeneity of the IPN. The long time behavior of the particle is characterized by an activated process associated to the motion between cells. This suggests that the potential energy related to the variable $\mathbf{R}$ may be characterized, in a first approximation, by a periodic potential:

$$U_R(\mathbf{R}) = U_0[1 - \cos(\mathbf{q}\cdot\mathbf{R})] \tag{8}$$

where $q = |\mathbf{q}| = 2\pi/\lambda$ and λ is an average characteristic length scale related to a mesh size in IPNs. Nevertheless, the dynamics of particles crossing cages can be considered as an activated process. Then, an analytical improvement can be made by approximating the potential U_R in terms of a bistable potential obtained expanding $\cos(\mathbf{q}\cdot\mathbf{R})$. Now, the complete potential entering in the Boltzmann factor can be written in the following form:

$$U(\mathbf{r},\mathbf{R}) \approx 1/2k_R(\mathbf{R})\mathbf{r}^2 + U_0\left[\frac{(\mathbf{q}\cdot\mathbf{R})^2}{2} - \frac{(\mathbf{q}\cdot\mathbf{R})^4}{24}\right] \tag{9}$$

Using eqs 4−6, it is possible to show that the mesoscopic entropy production per unit volume σ in the system is of the form

$$\sigma(t) = -k_B(\mathbf{v}_r f)\cdot\frac{\partial}{\partial \mathbf{r}}\ln\left[\frac{f}{f_{leq}}\right] - k_B(\mathbf{V}_R f)\cdot\frac{\partial}{\partial \mathbf{R}}\ln\left[\frac{f}{f_{leq}}\right] \tag{10}$$

Using $f_{leq}(\mathbf{r},\mathbf{R})$ given in eq 6 and the chemical potential $\mu = k_B T \ln|f/f_{leq}|$, and assuming a linear relationships between forces and currents in eq 10, i.e., $\mathbf{v}_r = -\beta(t)\nabla_r\mu$ and $\mathbf{V}_R = -\xi(t)\nabla_R\mu$, where $\beta(t)$ and $\xi(t)$ are Onsager coefficients,[38,40] it is easy to show that the nonequilibrium distribution function obeys the following Fokker−Planck type equation:

$$\frac{\partial f}{\partial t} = -\frac{\partial}{\partial \mathbf{r}}\cdot\left[k_B T\beta(t)\frac{\partial f}{\partial \mathbf{r}} + \beta(t) f\frac{\partial U}{\partial \mathbf{r}}\right] - \frac{\partial}{\partial \mathbf{R}}\cdot\left[k_B T\xi(t)\frac{\partial f}{\partial \mathbf{R}} + \xi(t) f\frac{\partial U}{\partial \mathbf{R}}\right] \tag{11}$$

The time dependence of $\beta(t)$ and $\xi(t)$ coefficients comes from the fact that we are dealing here with a slow non-Markovian processes. Hence, the time dependence takes into account memory effects, making eq 11 suitable for describing the anomalous diffusion of the microspheres as observed in the experiments presented here, as well as in others previously reported.[38,40,41]

The correlation between theory and experiment may be performed by analyzing the time evolution of the MSD of particles, through deriving evolution equations for the moments of the distribution function defined according to

$$\langle \mathbf{r}^j(t)\rangle \equiv \int f(\mathbf{r},\mathbf{R},t)\mathbf{r}^j\, d\mathbf{r}\, d\mathbf{R} \quad \text{and} \quad \langle \mathbf{R}^j(t)\rangle \equiv \int f(\mathbf{r},\mathbf{R},t)\mathbf{R}^j\, d\mathbf{r}\, d\mathbf{R} \tag{12}$$

where $j = 1, 2$. Performing a time derivative of eqs 12, employing eq 11, and partially integrating, we can give an expression for the moments through a set of coupled equations. The configurational variables $\mathbf{R}$'s and $\mathbf{r}$'s describe the slow fluctuations of the massive polymer cells and the fast fluctuations of the microspheres, respectively. Their time scales are quite separate. Therefore, we assumed that $f(\mathbf{r},\mathbf{R},t)$ can be expressed as a conditional probability of the form $f(\mathbf{r},\mathbf{R},t) = \varphi(\mathbf{R},t)\ \chi_R(\mathbf{r},t)$ and that $\langle k_R(R)\rangle = k_R(\langle \mathbf{R}\rangle)$. All these assumptions allow us to get the following set of coupled equations:

$$\frac{d}{dt}\langle \mathbf{r}\rangle = -\beta(t)k_R(\langle \mathbf{R}\rangle)\langle \mathbf{r}\rangle_R \tag{13}$$

$$\frac{d}{dt}\langle \mathbf{r}^2\rangle = 6k_B T\beta(t) - 2\beta(t)k_R(\langle \mathbf{R}\rangle)\langle \mathbf{r}^2\rangle_R \tag{14}$$

$$\frac{d}{dt}\langle \mathbf{R}\rangle = -\xi(t)U_0\mathbf{q}\left(\langle \mathbf{q}\cdot\mathbf{R}\rangle - \frac{\langle(\mathbf{q}\cdot\mathbf{R})^3\rangle}{6}\right) \tag{15}$$

$$\frac{d}{dt}\langle \mathbf{R}^2\rangle = 6k_B T\xi(t) - 2\xi(t)U_0\left(\langle(\mathbf{q}\cdot\mathbf{R})^2\rangle - \frac{\langle(\mathbf{q}\cdot\mathbf{R})^4\rangle}{6}\right) \tag{16}$$

Here, $\langle r\rangle_R = \int \chi_R(\mathbf{r})\mathbf{r}\, d\mathbf{r}$. Equation 14 can be integrated to yield the following expression:

$$\langle \Delta\mathbf{r}^2(t)\rangle = \frac{3k_B T}{k_R(\langle \mathbf{R}\rangle)}[1 - \exp(-2k_R(\langle \mathbf{R}\rangle)\int \beta(t')\, dt')] \tag{17}$$

Now, an expression for $k_R(\langle \mathbf{R}\rangle)$ can be obtained, assuming that the spring constant is isotropic with respect to $\mathbf{R}$, and that large fluctuations in $\mathbf{R}$ reduce its magnitude. Then, in a first approximation $k_R(\langle R\rangle) \approx k_0 - k_1\langle \Delta\mathbf{R}^2\rangle$, which introduced in eq 17 produces

dx.doi.org/10.1021/jp4105344 | J. Phys. Chem. B 2014, 118, 1146−1158

$$\langle \Delta \mathbf{r}^2(t) \rangle = \frac{2k_B T}{k_0}\left[1 + \frac{k_1}{k_0}\langle \Delta R^2 \rangle\right] \times [1 - \exp(-2k_0 \int \beta(t')\, dt')] \quad (18)$$

Because the MSD of a microsphere shows regions with a power law time dependence, we assumed a power law distribution of relaxation times compatible with the coefficient $\beta(t) = \delta_r \tau_r (t/\tau_r)^{\alpha-1}$.[38,40,41] Here, δ_r was added to make $\beta(t)$ be dimensionally correct. Thus, the time dependence for the integral function in eq 18 is

$$\int \beta(t')\, dt' = \frac{\delta_r {\tau_r}^2}{\alpha}\left[\left(\frac{t}{\tau_r}\right)^{\alpha} - \left(\frac{t_0}{\tau_r}\right)^{\alpha}\right] \quad (19)$$

where t_0 is a cutoff initial time; for short times it is essentially zero. Finally, we obtain

$$\langle \Delta \mathbf{r}^2(t) \rangle = \frac{3k_B T}{k_0}\left[1 + \frac{k_1}{k_0}\langle \Delta R^2 \rangle\right] \times \left[1 - \exp\left(-\frac{2k_0 \delta_r {\tau_r}^2}{\alpha}\left[\left(\frac{t}{\tau_r}\right)^{\alpha} - \left(\frac{t_0}{\tau_r}\right)^{\alpha}\right]\right)\right] \quad (20)$$

Equation 16 can also be explicitly integrated, but an algebraic transformation has to be performed, $dt = \xi^{-1} d\tau$, and the following integrals have to be introduced: $\int (\mathbf{q}\cdot\mathbf{R})^n f\, d\mathbf{r}\, d\mathbf{R} = q^n \int \mathbf{R}^n \cos^n \theta f\, d\mathbf{r}\, d\mathbf{R} = q^n \langle \bar{\mathbf{R}}^n \rangle$. These steps allowed us to obtain the expression

$$\frac{d}{d\tau}\langle \mathbf{R}^2 \rangle = 6k_B T - 2U_0 q^2\left(\langle \bar{\mathbf{R}}^2 \rangle - \frac{\langle \bar{\mathbf{R}}^4 \rangle}{6}\right) \quad (21)$$

Equation 21 can be reduced by calculating the time variation of $\langle (\mathbf{q}\cdot\mathbf{R})^2 \rangle$, using eq 11. This gives

$$\frac{d}{d\tau}\langle (\mathbf{q}\cdot\mathbf{R})^2 \rangle = 2k_B T q^2 - 2U_0 q^2 \langle (\mathbf{q}\cdot\mathbf{R})^2 \rangle + \frac{U_0 q^2}{3}\langle (\mathbf{q}\cdot\mathbf{R})^4 \rangle \quad (22)$$

Calculating explicitly the integrals for $\langle (\mathbf{q}\cdot\mathbf{R})^2 \rangle$ leads to the following equation:

$$\frac{d}{d\tau}\langle \bar{\mathbf{R}}^2 \rangle = 2k_B T - 2U_0 q^2 \langle \bar{\mathbf{R}}^2 \rangle + \frac{U_0 q^4}{3}\langle \bar{\mathbf{R}}^4 \rangle \quad (23)$$

Then, eqs 23 and 21 yield the following relation:

$$\langle \Delta \mathbf{R}^2 \rangle = \langle \Delta \bar{\mathbf{R}}^2 \rangle + 4k_B T \int_{t_0}^{t} \xi(t')\, dt' \quad (24)$$

In an equivalent way as before, we may also assume a power law distribution of relaxation times for the coefficient $\xi(t) = \delta_R (t/\tau_R)^{\varepsilon-1}$, with an exponent ε and characteristic time τ_R.[38,40,41] A final expression for eq 24 can be obtained by solving eq 23 through direct integration, and by using the Gaussian decoupling $\langle \bar{\mathbf{R}}^4 \rangle \approx \langle \bar{\mathbf{R}}^2 \rangle \langle \bar{\mathbf{R}}^2 \rangle$.[42] This gives the following result:

$$\langle \Delta \bar{\mathbf{R}}^2 \rangle = \frac{3}{q^2}\left[1 + \Psi \tan\left(\Psi U_0 q^2 \int_{t_0}^{t} \xi(t')\, dt' - \arctan\left(\frac{1}{\Psi}\right)\right)\right] \quad (25)$$

where $\Psi = (2k_B T/3U_0 - 1)^{1/2}$. Now, expanding the tangent function to the first order to avoid its divergences, a smoother function of time can be obtained. Then, inserting eq 25 into eq 24, a final expression for $\langle \Delta \mathbf{R}^2 \rangle$ can be written as

$$\langle \Delta \mathbf{R}^2 \rangle = \frac{3}{q^2}\left[1 - \Psi \arctan\left(\frac{1}{\Psi}\right)\right] + [6k_B T - 3U_0]\left(\frac{\delta_R \tau_R}{\varepsilon}\left[\left(\frac{t}{\tau_R}\right)^{\varepsilon} - \left(\frac{t_0}{\tau_R}\right)^{\varepsilon}\right]\right) \quad (26)$$

The total expression for the mean square displacement of a particle can be written, in a first approximation, as $\langle \Delta \boldsymbol{\rho}^2(t) \rangle = \langle \Delta \mathbf{R}^2(t) \rangle + \langle \Delta \mathbf{r}^2(t) \rangle$, that is

$$\langle \Delta \rho^2(t) \rangle = \frac{3}{q^2}\left[1 - \Psi \arctan\left(\frac{1}{\Psi}\right)\right] + [6k_B T - 3U_0]\left[\frac{\delta_R \tau_R}{\varepsilon}\right]\left[\left(\frac{t}{\tau_R}\right)^{\varepsilon} - \left(\frac{t_0}{\tau_R}\right)^{\varepsilon}\right] + \frac{3k_B T}{k_0}\left[1 + \frac{k_1}{k_0}\langle \Delta R^2 \rangle\right] \times \left[1 - \exp\left(-\frac{2k_0 \delta_r {\tau_r}^2}{\alpha}\left[\left(\frac{t}{\tau_r}\right)^{\alpha} - \left(\frac{t_0}{\tau_r}\right)^{\alpha}\right]\right)\right] \quad (27)$$

The final expression given by eq 27 can be used to fit our experimental data for particles fluctuating in an IPN. The fitting allows us to estimate several properties of the network−particle interaction, such as the spring coefficients, k_0 and k_1, the average mesh size, and the height of the periodic potential representing an IPN, λ and U_0, as well as the constants and exponents characterizing the memory functions. It is important to note that in this model an explicit polymer dynamics was not used, which is an attractive feature of the model. Polymer dynamics is hidden in the functional form of the memory functions, in the elastic form of the first term of the interaction potential, and in the parameter α that describes the particle's dynamics at short times.

4. RESULTS

4.1. MSD during Polymerization. MSDs of microspheres embedded in the slightly interconnected polymer networks were obtained by using the DWS. Figure 2 presents typical examples of the measured MSD vs time curves as a function of elapsed time since the polymerization reaction started, for the particles immersed in the polymeric solution. The examples have different cross-linker concentrations: %C = 0.0 (Figure 2a), 0.5 (Figure 2b), and 1.0 (Figure 2c), but the same total polymer concentration, %P = 6.6. Experimental data can be approximated in limited ranges of time by $\langle \Delta \boldsymbol{\rho}^2(t) \rangle \sim t^{\kappa}$. Usually, $\kappa = 1$ at short time scales ($t \to 0$) as well as at long time scales ($t \to \infty$); $\kappa < 1$ at intermediate time scales. Our measured MSD curves can be similar to anomalous diffusion, if measurements just cover intermediate time scales. Anomalous diffusion is a process where $\langle \Delta \boldsymbol{\rho}^2(t) \rangle \sim t^{\kappa}$, with $\kappa \neq 1$ (κ being the slope of the log−log plot of the MSD vs t). This is a diffusion behavior common in disordered and fractal structures.[44,48]

dx.doi.org/10.1021/jp4105344 | J. Phys. Chem. B 2014, 118, 1146−1158

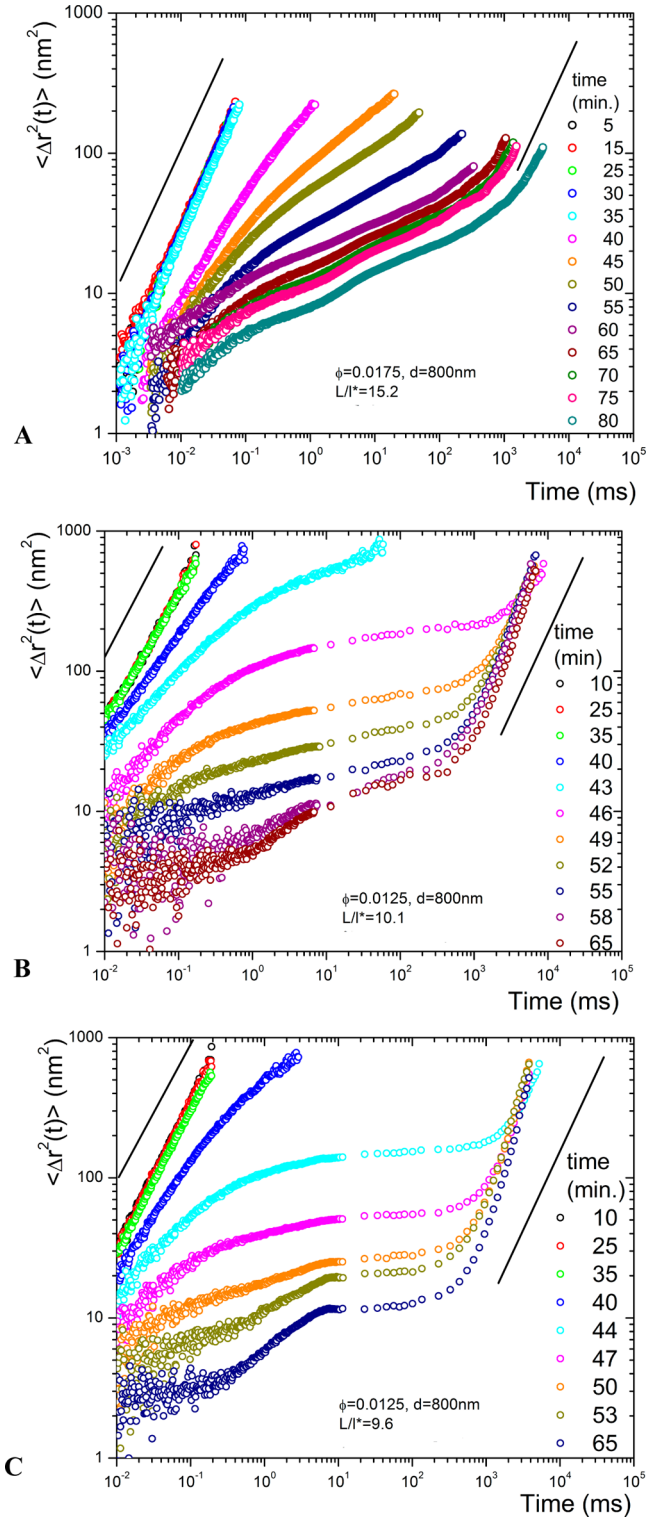

Figure 2. Typical examples of the MSD vs time curves for microspheres (diam = 800 nm), as the polymerization reaction progresses. The legend is the elapsed time since polymerization started. In all of them %P = 6.6. A) %C = 0.0 and %T = 0. B) %C = 0.5 and %T = 0.033. C) %C = 1.0 and %T = 0.066. Straight lines have a slope = 1 corresponding to $\langle \Delta \boldsymbol{\rho}^2(t) \rangle \sim t$.

For the case of particles embedded in a polymer mixture that will not develop cross-links, a diffusive regime $\langle \Delta \boldsymbol{\rho}^2(t) \rangle \sim t$ is observed (Figure 2a) at early stages of the polymerization process; viscosity of the polymeric solution remains still close to pure water. Later, ∼40 min, the particle dynamics is diffusive at short times, but at longer times it is subdiffusive; the κ exponent decreases as the polymer chains are formed. The time interval where motion is diffusive decreases quite fast as the polymerization reaction advances. These observations suggest that the formation of polymer chains induces strong interactions with the microspheres, through the formation of loose cages that allow Brownian particles to escape after network relaxation. These interactions are responsible for having exponents $\kappa < 1$.[41] The change of particle dynamics, during the polymerization reaction, is similar to the evolution of the MSD of particles when the polymer concentration increases in polymer networks without cross-links.[49,50] The behavior for the fully polymerized network illustrated in Figure 2a is similar to that found in PEO solutions by Dasgupta et al.;[32] there, the particle MSD curves were fitted with a two-step power law.

For the case of a polymer mixture with a small quantity of cross-linkers (Figure 2b,c), two dynamic regimes become quite visible in the MSD curves when the reaction time is ∼43 min. At short times, the diffusion is still subdiffusive. However, at larger times a big shoulder appears that extends for a couple of orders of magnitude in time, forming a kind of small plateau. This behavior is different from the case of polymerization without cross-linkers, %C = 0 (Figure 2a). For subsequent stages of the polymerization reaction with cross-linkers, three different regimes for particle motion can be observed. At the very short times (<10 ms), the behavior of $\langle \Delta \boldsymbol{\rho}^2(t) \rangle$ corresponds to a subdiffusive regime. In advanced stages of the polymerization process these MSD curves can be very noisy; this is due to the short time window for correlation measurement. At intermediate times around 10−1000 ms, $\langle \Delta \boldsymbol{\rho}^2(t) \rangle$ remains almost constant for a given time interval (a plateau); this is more marked for the case of %C = 1 (Figure 2c). At these time scales, particles apparently explore all the available volume of the cage surrounding them formed by the polymer network; clearly, cross-linkers restrict the motion of particles in an important way. At longer times (∼1000 ms), particles apparently find the way out of the constraining cages. In spite of the cross-links, the network can relax and there are enough network fluctuations for allowing particles to escape. The MSD curves present an enhanced diffusion regime $\langle \Delta \rho^2(t) \rangle \sim t^{\kappa}$ with $\kappa > 1$; for simplicity we will call this motion "superdiffusive" from now on. The simplest argument to explain why particles present an enhanced diffusion is because the network has not relaxed after the polymerization process apparently ended up; there are residual slowly relaxing stresses created during the polymerization. When particles interact with the not relaxed polymer network, a remnant stress in the network makes particles move slightly faster than in the simple diffusive case. This explanation is consistent with a previous calculation[41] in which the exponent κ of the MSD has been related with the main oscillation mode ω_0 of the network: $\kappa \sim 1/\omega_0^2$. Relaxed networks are stiffer; consequently, they have larger ω_0 values and therefore lower exponents. On the contrary, nonrelaxed networks are weaker due to large thermal fluctuations. Therefore, they have lower characteristic oscillation modes and present higher κ exponents. Another possibility could be that superdiffusive motion might be apparent, due to convective motion related to nonuniform temperature gradients in the samples; we do not consider that this is happening in our experimental setup.

4.2. Hydrolysis and Shrinking of the Slightly IPN. The resulting slightly IPNs from the polymerization of acrylamide

dx.doi.org/10.1021/jp4105344 | J. Phys. Chem. B 2014, 118, 1146−1158

and bisacrylamide, with embedded microspheres, were partially hydrolyzed in a basic aqueous solution of TEMED for 2 days, as mentioned above. Prior to shrinking the samples, by immersing them in acetone–water solutions, it was considered interesting to know how the MSD of microspheres evolves in time in hydrolyzed polymeric networks. As far as we know, there is no such kind of measurements. Figure 3 presents the

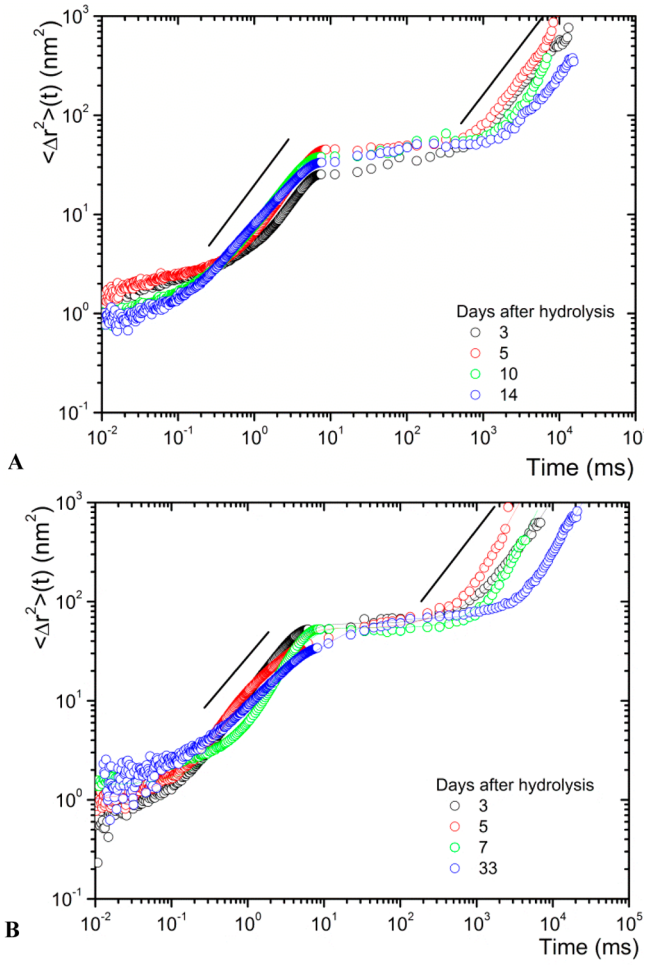

Figure 3. Two examples of MSD vs time curves for microspheres embedded in the hydrolyzed polymer network several days after hydrolysis has finished. Lines with experimental data are guides to the eye and straight lines have a slope = 1 corresponding to $\langle \Delta\rho^2(t) \rangle \sim t$.

MSD vs t curves for microspheres in a couple of samples of hydrolyzed IPNs as a function of the elapsed time since the hydrolysis process ended, both with the same polymer concentration and hydrolysis time. The MSD curves for the embedded microspheres are quite similar, and they show almost the same features no matter how much time after the hydrolysis has elapsed. However, it is clear that polymer network relaxation takes a long time after the hydrolysis process has finished, because the curves present small changes, although without any specific trend; apparently, each IPN relaxed through a different pathway. In Figure 3, at very short times the $\langle \Delta\rho^2(t) \rangle$ is quite noisy. After approximately a couple of decades in time, motion is diffusive, $\langle \Delta\rho^2(t) \rangle \sim t$. Then, there is a small plateau at longer times, which extends approximately over two decades in time. At long times $\langle \Delta\rho^2(t) \rangle \sim t$, i.e., the particle motion becomes approximately diffusive again. Here, in contrast to the case of the polymerization process, a considerable time has elapsed since polymerization and hydrolysis have ended. Here, when particles interact with the relaxed polymer network, they move as in the simple diffusive case.

4.2. MSD at Different Swelling Fractions. A group of samples of acrylamide, bisacrylamide, and water, with the embedded microspheres that were also hydrolyzed in a TEMED solution for 48 h, were submerged in acetone–water mixtures for another 48 h to reach a new equilibrium volume (water: 100–55 wt %). Depending on the time the polymer gel was allowed to hydrolyze, it will change its volume in a definite way when equilibrated with a acetone–water solution;[1] in all the cases our gels contracted. The change in volume may be continuous or discontinuously depending on the acetone–water concentration (above or below the critical point). We preferred to work in the case of continuous volume change to have more control on the experiments to be described below. In Figure 4, we present a typical example of diagram of acetone–water concentration vs swelling ratio (final volume/initial volume) for a slightly IPN that was hydrolyzed for 2 days.

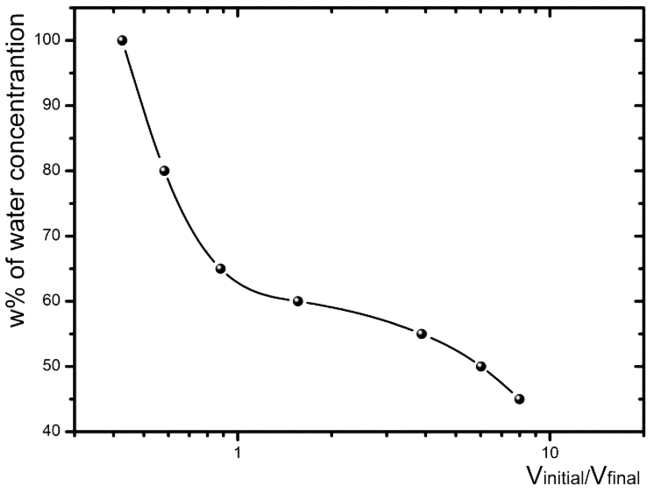

Figure 4. Typical diagram of concentration of the acetone–water solution where previously hydrolyzed IPN were immersed vs swelling ratio reached after two days of immersion.

Figure 5 presents typical MSD vs time curves for particles embedded in a shrunken partially ionized IPN (%P = 6.6%, %C = 2%) as a function of time after subsequent volume contractions; each curve corresponds to a specific percent of volume shrinking. A specific contracted volume was obtained by equilibrating the partially ionized IPN in an acetone–water mixture for 72 h with the appropriate concentration (as in Figure 4). All the curves present three regimes. At short times, particles move subdiffusively, i.e., $\langle \Delta\rho^2(t) \rangle \sim t^{\kappa}$, where $\kappa \sim$ 0.4–0.6. At intermediate times, $\langle \Delta\rho^2(t) \rangle$ presents a plateau extending approximately over 2 orders of magnitude. At these time scales, cross-linkers and the less available volume restrict the motion of particles. Apparently, particles are trapped and explore all the available volume of the polymer network cage formed around them, before to find a way out. In spite of the cross-links and volume reduction, the network can relax and there are enough network fluctuations for allowing the Brownian particles to escape. Depending on the case, particles present diffusive motion, or superdiffusive motion. When the

dx.doi.org/10.1021/jp4105344 | J. Phys. Chem. B 2014, 118, 1146–1158

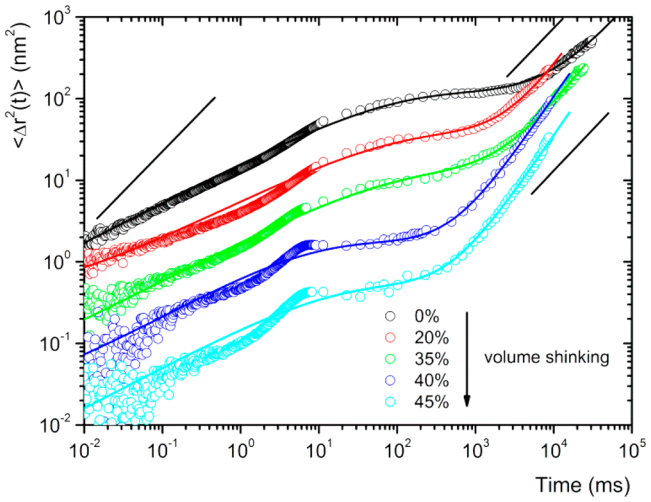

Figure 5. MSD vs t as a function of the volume shrinking for particles (diam 600 nm) embedded in partially ionized IPN with %P = 6.6%, %C = 2%, and %T = 0.132. The polymer network was shrunk successively by allowing equilibration with different acetone−water mixtures (100−55%) for 72 h; the less water in the mixture, the larger the shrinking. Lines are the best fit-curves calculated with the model eq 27 to the experimental points. Straight lines have a slope = 1 corresponding to $\langle \Delta\boldsymbol{\rho}^2(t) \rangle \sim t$.

IPNs are equilibrated with solutions rich in water (80−100%), the network apparently is structurally relaxed at long times. Particle motion is diffusive, $\langle \Delta\boldsymbol{\rho}^2(t) \rangle \sim t$, probably because they were not submitted to excessive shrinking. For the case of IPNs that were significantly shrunk with acetone−water solutions at 55% and 60% (volume shrinking >40%), there is a short time interval where motion is close to diffusive before reaching the plateau; this is reached through a pronounced change of curvature; a kind of pronounced kink. This unexpected behavior is more pronounced as the IPNs undergo larger volume contractions. Here, the most probable explanation is that IPNs have not yet relaxed completely. Here, $\langle \Delta\boldsymbol{\rho}^2(t) \rangle \sim t^{\kappa}$ with $\kappa > 1$. As discussed before, when particles interact with a not-relaxed polymer network, apparently a remnant stress in the network makes particles move slightly faster than in the simple diffusive case. A more abrupt volume change requires longer relaxation times to reach a structural equilibrium, and $\langle \Delta\boldsymbol{\rho}^2(t) \rangle$ apparently can detect this condition. In the case of samples reaching even larger shrinking volumes, not discussed here, they turn out to be white, revealing regions with large concentration fluctuations of a size to allow light scattering. These samples needed months to be completely transparent, revealing a very slow relaxation process. In Figure 5, the best fit curves to the experimental MSDs are also presented; they were calculated with the model described by eq 27, in section 3. For the case of the partially ionized polymer networks that were not submitted to excessive shrinking, the fitting is quite good. For the case of the IPNs that were significantly shrunk, the fitting is good in general, although they do not fit well in the region before reaching the plateau, that is, where particle motion is close to diffusive motion and in the pronounced change of curvature.

An additional feature of the model is that the fitting parameters can be physically interpreted. Figure 6 presents the time evolution of some of the fitting parameters as a function of the polymerization time for the curves presented in Figure 2b,c; only for the cases with a very good fitting were used. Here, the

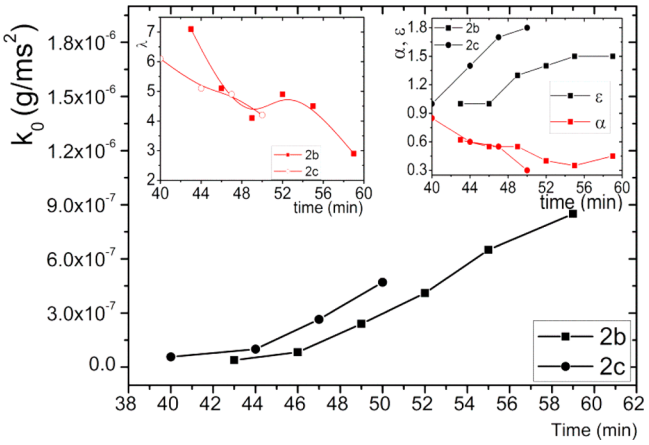

Figure 6. Time evolution of the parameters of our model during the polymerization reaction, for the examples presented in Figure 2b,c. Main figure k_0 vs time. Left inset presents the evolution of λ (nm). Right inset presents the evolution of the exponents α and ε. Lines are guides to the eye.

elastic constant k_0, related to the interaction of the particle with the elements of the polymer network, increases in a sigmoidal form as the polymerization advances. As expected, this parameter captures the fact that the polymer is stiffer as the polymerization advances, reaching an almost constant value around 60 min. In one of the insets of Figure 6, we present the evolution of the parameter λ associated with the average periodicity of the polymer network of the IPN. λ decreases as the polymerization advances, in agreement with what would be expected if both the size of the acrylamide polymer chains and the number of bisacrylamide links grow. In another inset of Figure 6, the evolution of the exponents α and ε is presented. α, the exponent related to the motion of particles at short times, decreases as the polymerization advances; the motion of the microspheres is subdiffusive. At short times, the MSD captures the dynamics of the short length scales of the polymer network. A decrease in α exponent means that the local relaxation process is changing as polymerization advances. This evolution in the short length scales stops ∼52 min after the polymerization has started. It remains relatively constant even when the ε exponent is changing. The ε exponent is related to the motion of the particle at long times and longer scales; it is directly related to the properties and fluctuations of the IPN, as follows from eqs 20, 26, and 27. ε increases as the polymerization advances, revealing the nonequilibrated structural relaxation of the IPN. We discussed this behavior above.

For the case of successive shrinking, Figure 7 presents how the parameters of the model change as a function of the swelling ratio, $V_{\text{initial}}/V_{\text{final}}$. The constant of force k_0 increases linearly with the swelling ratio; as the volume contracts, the polymer network becomes stiffer. This is in agreement to what we observe with the polymer network as it shrinks. In one of the insets of Figure 7, we present the change of the average periodicity, λ, which decreases in the first shrinking steps, but apparently it reaches a plateau where its change is negligible as the IPN contracts. In a simple model of Brownian particles harmonically bound around a stationary mean position, the MSD can be modeled as[41,43] $\langle \Delta\mathbf{r}^2(t) \rangle = 6\delta^2(1 - e^{-(D_0/\delta^2)t})$, where D_0 is the short time diffusion and δ is the particle's amplitude motion, i.e., the cage size. δ is also related to the plateau modulus G_0 ($\delta^2 = k_BT/[6\pi aG_0]$).[43] For comparison

dx.doi.org/10.1021/jp4105344 | J. Phys. Chem. B 2014, 118, 1146−1158

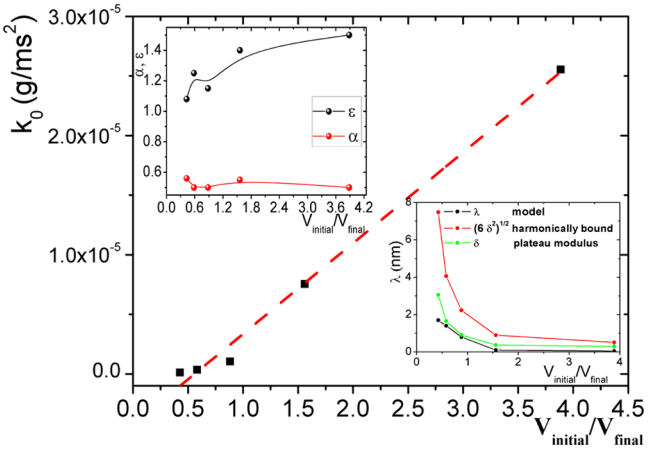

Figure 7. Parameters of our model as a function of the successive volume reductions for the example in Figure 5. Main figure k_0 vs $V_{initial}/V_{final}$, the red dashed line is the best fit to the data. The right inset presents the change of λ (nm) vs $V_{initial}/V_{final}$. For comparison, it was included the amplitude for a particle harmonically bound around a stationary mean position obtained fitting the MSD data, and δ calculated from G_0 (see text). Left inset presents the change of the exponents α and ε. Lines are guides to the eye.

with λ, both the particle's amplitude obtained fitting the MSD data to the given formula and the δ coming from G_0 were included in the inset; G_0 can be calculated with the result of the next section. These simple ways for obtaining a cage size behave in the same manner as the λ.

In another inset of Figure 7, the exponents are plotted as a function of the swelling ratio. The α exponent essentially does not change. As the polymer network contracts stepwise, the size of the cage decreases. However, the motion at short times is always subdiffusive with $\kappa \sim 1/2$. As discussed above, the local structure apparently remains the same, and the local relaxation process is not changing. The ε exponent is close to one when the network volume reduction is not large, but it increases when the volume of the polymer network is importantly reduced; here, motion is superdiffusive, and as mentioned above the network has not relaxed.

4.3. Elastic and Viscous Modulus. Viscoelastic spectra were evaluated from the MSD vs t curves for the two types of IPNs of interest here: For those obtained both during the polymerization process (Figure 2b) and from each step after subsequent volume contractions (Figure 5). The viscoelastic spectra were obtained through eq 3, evaluating the logarithmic derivative of best fitting curves for MSD vs t data; the fitting curves were based on the theoretical model described before. It is important to take into consideration that the agreement between DWS and mechanical rheology is in general good, although it is not excellent.[43,51] Trends and features are identical, but the actual numerical values differ a little. Comparison of rheological data obtained by different methods is not an easy task because protocols play a central role, as well as cell geometry, cell parameters, sample preparation, etc. DWS microrheology seems to share some of these problems; here it is critical to ensure that particle aggregation is not occurring during measurements. The l^* measurement is a useful tool, because it is very sensible to detect particle aggregation. It is also important to recall that for the case of the polymerization process, the method employed here to get rheological information perturbs the polymerization reaction and the newly formed network in a minimum level. From $G'(\omega)$ and $G''(\omega)$ in Figure 8a, the values of both viscoelastic moduli increase as far the polymerization advances. In general, the

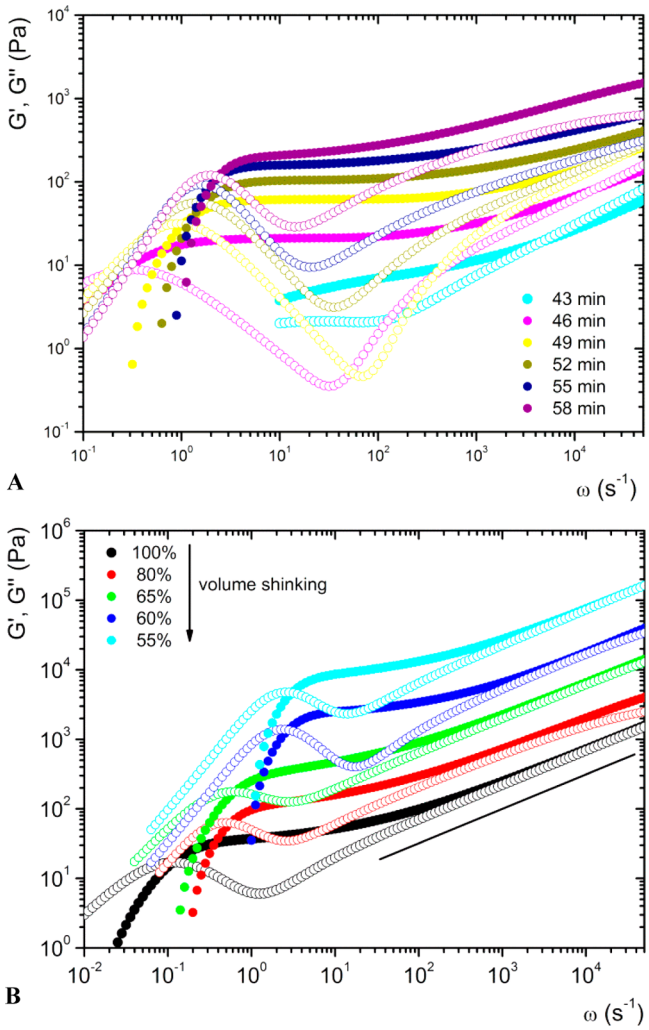

Figure 8. $G'(\omega)$ (filled circles) and $G''(\omega)$ (hollow circles). (A) Moduli calculated from the MSD during the polymerization process. (B) Moduli for an IPN as a function of the volume shrinking, for %P = 6.6%, %C = 2%, and %T = 0.132 . The polymer network was shrunk successively by allowing equilibration with different acetone−water mixtures (100−55%) for 72 h; the less water in the mixture, the larger the shrinking. The black straight line has a slope = 1/2 corresponding to $G''(\omega)$ and $G'(\omega) \sim \omega^{1/2}$.

IPNs are more viscous at low frequencies and, at larger frequencies, after a crossing point, the sample is more elastic. Also, the crossover frequency increases as polymerization advances, except for the early stages of polymerization (t = 43 min). The frequency corresponding to the bottom of the well for the viscous modulus at intermediate frequencies decreases as the polymerization reaction evolves. Because $\langle \Delta\boldsymbol{\rho}^2(t) \rangle$ is noisy at short times, due to the short time window for the correlation measurement, probably the past decade at high frequencies is not accurate.

In the second case, the volume of the IPN was successively contracted (Figure 8b). At low frequencies the IPN is more viscous, $G''(\omega) > G'(\omega)$, and after a crossing point it is more elastic $G''(\omega) < G'(\omega)$. As far as the IPN is stepwise shrunk, the values of both viscoelastic moduli increase, and both $G'(\omega)$ and $G''(\omega)$ curves move to higher frequencies. At high frequencies,

dx.doi.org/10.1021/jp4105344 | J. Phys. Chem. B 2014, 118, 1146−1158

both moduli follow a power law behavior, i.e., $G''(\omega)$ and $G'(\omega) \sim \omega^s$, with s in the range 0.4−0.6. Notice that these results seem to be consistent with a Rouse-like relaxation showing an exponent $\kappa \sim 1/2$.[42] This is a direct consequence of the measured values for the MSD at short times. The viscoelastic moduli shown in Figure 8 are reminiscent of those obtained in systems with embedded thread-like structures, as with worm-like micelles,[43,45] fd virus,[46] and actine,[47] although their short length relaxation dynamics at higher frequencies differ, due to their particular characteristics. In both cases, polymerization and shrinking, a crossover between $G''(\omega)$ and $G'(\omega)$ is found at low frequencies, and the elastic modulus presents a kind of plateau. However, a question can be posed. If we have interconnected networks, why do the curves of $G'(\omega)$ and $G''(\omega)$ cross each other? One would expect that the crossover frequency decreases as polymerization goes on, which is not the case here. This can be explained by taking into account that we are dealing with a very slightly interconnected network immersed in water. As shown by Dasgupta and Weitz,[32] a Brownian particle moving in a polymer network without cross-links can be described by a two-step power law with exponents around 0.4 and 0.9, at short and long times, respectively. This is similar to our case for the MSD presented in the inset of Figure 9a for one of the cases described in Figure 2a. This MSD produces the moduli presented in Figure 9a. Here at low frequencies, a crossover frequency is present, but there is no plateau. In contrast, in a highly interconnected network, a colloidal particle moves subdiffusively for a couple of decades, before being completely trapped in a cage. This leads to a plateau that extends indefinitely (see inset of Figure 9c); there is no finite longest relaxation time. This behavior has also been observed previously with microrheology.[7] Therefore, a highly interconnected gel is characterized by an elastic modulus larger than the viscous modulus. Polymer relaxation dynamics in gels can be translated to the moduli behavior at very high frequencies (Figure 9c) transforming the MSD; we evaluated the moduli from the MSD given in the inset of Figure 9c. Our experiments with slightly interconnected networks are located between a polymer network without any interconnection and a polymer gel with too many connections. In the slightly interconnected polymers networks, the Brownian particle presents a small plateau that extends only for one or two decades, but at longer times, the particles can escape from the cages. In this particular case, a crossover frequency is present at low frequencies in the moduli, and a plateau is formed before reaching the short length relaxation dynamics at higher frequencies (Figure 9b). Figure 9 as a whole gives insight into the formation of a highly elastic interconnected network. First, it starts with a polymer network without interconnections. Then, when a small amount of cross-links is added where the elastic contribution increases, a plateau is formed at intermediate frequencies. A small number of cross-links induces the formation of cages, trapping the Brownian particle for a period of time. Further addition of cross-links increases the elasticity of the gel, shifting the crossover frequency to higher frequencies. At some point, the particle cannot escape from the cages formed by the interconnected network, and the crossover in the moduli is lost. Then, a big plateau is formed in the elastic modulus. Rouse-like relaxation dynamics is still present at higher frequencies in the viscoelastic spectra, which remains almost unaltered; the local relaxation processes is not affected by the network cross-link density.

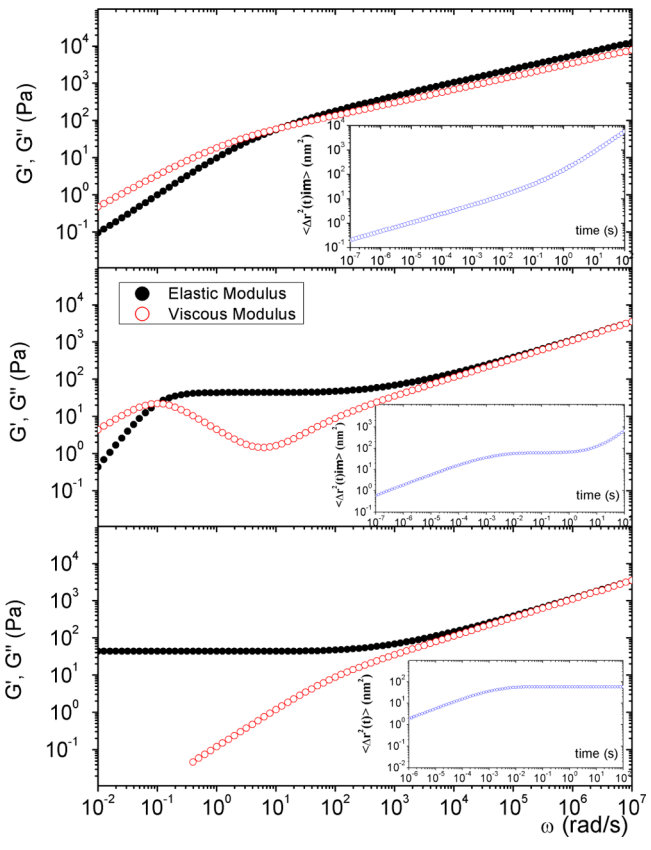

Figure 9. Moduli behavior of polymer networks as the number of cross-links increases. Upper panel: polymer without cross-links; inset, MSD vs t. Middle panel: IPNs with a very small number of cross-links; inset MSD vs t. Lower panel: highly cross-linked polymeric gels; inset data of MSD vs t from ref 32.

5. CONCLUSIONS

In this article, we have performed a study involving experiments and theory about the MSD and about the viscoelastic properties of an interconnected polymer network when the number of interconnections is very low. We examined two cases, when the network is building up, that is, when polymerization is taking place, and when it is shrinking in a controlled way. The study was performed by using DWS measurements to obtain the MSD as a function of time for tracer microspheres embedded in the polymer network that is immersed in a solvent. The results were interpreted with a theoretical model of constrained diffusion based on a Fokker−Planck equation. The conjunction of these two approaches allowed us to determine, under the different physicochemical conditions imposed on the slightly interconnected polymer network, the trend of several physical parameters characterizing the system, namely, the elastic constant of the polymer network, the cage size, and the exponents determining the time evolution of the MSD. A better understanding of the processes influencing the time dependence behavior of the MSD provided a better understanding of the frequency behavior of $G^*(\omega)$, for the different stages of building up the network and for the swollen states of the polymer network.

We conclude that a rapid polymerization leads to nonequilibrated polymer networks that store energy through remnant stresses at short times, producing (together with the

dx.doi.org/10.1021/jp4105344 | J. Phys. Chem. B 2014, 118, 1146−1158

caging effect) subdiffusion. This remnant elastic energy is apparently liberated at long times, where an enhanced diffusion regime is observed. Similar behavior is observed for interconnected polymer networks subjected to important shrinking. Long structural relaxation times were associated with the anomalous diffusion observed in this case.

A general insight of the consequences of cross-link formation on the dynamics of embedded particles has been presented; thanks to a comparison of our results with those in a polymer without cross-links and in a polymer gel. The appearance of cross-links induces the formation of cages, in which the particles are trapped. This leads to an increase of the elastic modulus of the system. However, at small cross-link concentrations particles can escape from the cages, giving rise to a crossover in the viscoelastic spectra. Further addition of cross-links requires longer relaxation times, particles require more time to escape from the confining cages up to the point to be completely trapped. Then, cross-links lead to the formation of an extended plateau in the elastic modulus, characteristic of polymeric gels without a crossover in the viscoelastic spectra.

AUTHOR INFORMATION

Corresponding Author

*R. Castillo: e-mail, rolandoc@fisica.unam.mx.

Notes

The authors declare no competing financial interest.

ACKNOWLEDGMENTS

We thank C. Garza for his technical support. Funding from SEP-CONACYT (81081) and DGAPA-UNAM (IN 104911-3 and ID-100112-2) is gratefully acknowledged.

REFERENCES

(1) Tanaka, R.; Fillmore, D.; Sung, S. T.; Nishio, I.; Swislow, G.; Shah, A. Phase transitions in ionic gels. *Phys. Rev. Lett.* **1980**, *45*, 1636.

(2) Tanaka, T. Phase Transitions of Gels. In *Polyelectrolyte Gels*; ACS Symposium Series No. 480; American Chemical Society: Washington, DC, 1992; Chapter 1, p 1−21.

(3) Pekan, O.; Kara, S. Swelling of acrylamide gels made at various onset temperatures: an optical transmission study. *Polym. Int.* **2003**, *52*, 676.

(4) Doi, Y.; Tokita, M. Friction Coefficient and Structural Transition in a Poly(acrylamide) Gel. *Langmuir.* **2005**, *21*, 9420.

(5) Calvet, D.; Wong, J. Y.; Giasson, S. Rheological monitoring of PAAm hydrogel gelation: Importance of cross-link density and temperature. *Macromolecules* **2004**, *37*, 7762.

(6) Dasgupta, B. R.; Weitz, D. A. Microrheology of cross-linked polyacrylamide networks. *Phys. Rev. E* **2005**, *71*, 21504.

(7) Larsen, T. H.; Furst, E. M. Microrheology of the liquid-solid transition during gelation. *Phys. Rev. Lett.* **2008**, *100*, 146001.

(8) Larsen, T. H.; Schultz, K.; Furst, E. M. Hydrogel microrheology near the liquid-solid transition. *Korean-Australia Rheol. J.* **2008**, *20*, 165.

(9) Hames, B. D., Ed. *Gel Electrophoresis of Proteins*, 3rd ed.; Oxford University Press: New York, 1998.

(10) Masaro, L.; Zhu, X. X. Physical models of diffusion for polymer solutions, gels and solids. *Prog. Polym. Sci.* **1999**, *24*, 731.

(11) Johansson, L.; Elvingson, C.; Lofroth, J. E. Diffusion and interaction in gels and solutions. 3. Theoretical results on the obstruction effect. *Macromolecules* **1991**, *24*, 6024.

(12) Netz, P. A.; Dorfmüller, T. Computer simulation studies of diffusion in gels: Model structures. *J. Chem. Phys.* **1997**, *107*, 9221.

(13) Saxton, M. J. Anomalous diffusion due to obstacles: a Monte Carlo study. *Biophys. J.* **1994**, *66*, 394.

(14) Scheffold, F.; Romer, S.; Cardinaux, F.; Bissig, H.; Stradner, A.; Rojas-Ochoa, L. F.; Trappe, V.; Urban, C.; Skipetrov, S. E.; Cipelletti, L.; Schurtenbeger, P. New trends in optical micro-rheology of complex fluids and gels. *Prog. Colloid Polym. Sci.* **2004**, *123*, 141.

(15) Waigh, T. A. *Rep.* Microrheology of complex fluids. *Prog. Phys.* **2005**, *68*, 685.

(16) Cicuta, P.; Donald, A. M. Microrheology: a review of the method and applications. *Soft Matter.* **2007**, *3*, 1449.

(17) Willenbacher, N.; Oelschlaeger, C. Dynamics and structure of complex fluids from high frequency mechanical and optical rheometry. *Curr. Opin. Colloid Interface Sci.* **2007**, *12*, 43.

(18) Squires, T. D.; Mason, T. G. Fluid Mechanics of Microrheology. *Annu. Rev. Fluid Mech.* **2010**, *42*, 413.

(19) Gardel, M. L.; Valentine, M. T.; Weitz, D. A. Microrheology. In *Microscale Diagnostic Techniques*; Breuer, K. S., Ed.; Springer: Berlin, 2005; Chapter 1, p 1.

(20) Lopez-Diaz, D.; Castillo, R. Microrheology of solutions embedded with thread-like supramolecular structures. *Soft Matter.* **2011**, *7*, 5926.

(21) Calvet, D.; Wong, J. Y.; Glasson, S. Rheological monitoring of polyacrylamide gelation: Importance of cross-link density and temperature. *Macromolecules* **2004**, *37*, 7762.

(22) Dıaz-Leyva, P.; Perez, E.; Arauz-Lara, J. L. Dynamic light scattering by optically anisotropic colloidal particles in polyacrylamide gels. *J. Chem. Phys.* **2004**, *121*, 9103.

(23) Dıaz-Leyva, P.; Perez, E.; Arauz-Lara, J. L. Brownian motion of optically anisotropic particles in weak polymer gels. *Rev. Mex. Fis.* **2004**, *50*, 633.

(24) Weitz, D. A.; Pine, D. J. Diffusing-Wave Spectroscopy. In *Dynamic Light Scattering*; Brown, W., Ed.; Oxford University Press: New York, 1993; Chapter 16, p 652.

(25) Pine, D. J.; Weitz, D. A.; Zhu, J. X.; Herbolzheimer, E. Diffusing-wave spectroscopy: Dynamics light scattering in the multiple scattering limit. *J. Phys. (Paris)* **1990**, *51*, 2101.

(26) Kaplan, D. D.; Kao, M. H.; Yodh, A. G.; Pine, D. J. *Appl. Opt.* **1993**, *32*, 3828.

(27) Mason, T. G. Particle tracking microrheology of complex fluids. *Phys. Rev. Lett.* **1997**, *79*, 3282.

(28) Gardel, M. L.; Valentine, M. T.; Weitz, D. A. Microrheology. In *Microscale Diagnostic Techniques*; Breuer, K. S., Ed.; Springer: Berlin, 2005; Chapter 1, p 1.

(29) Mason, T. G.; Weitz, D. A Optical Measurements of Frequency-Dependent Linear Viscoelastic Moduli of Complex Fluids. *Phys. Rev. Lett.* **1995**, *74*, 1250.

(30) Mason, T. G. Estimating the viscoelastic moduli of complex fluids using the generalized Stokes-Einstein equation. *Rheol. Acta* **2000**, *39*, 371.

(31) van Zanten, J. H.; Rufener, K. P. Brownian motion in a single relaxation time maxwell fluid. *Phys. Rev. E* **2000**, *62*, 5389.

(32) Dasgupta, B. R.; Tee, S. Y.; Crocker, J. C.; Frisken, B. J.; Weitz, D. A. Microrheology of polyethylene oxide using diffusing wave spectroscopy and single scattering. *Phys. Rev. E* **2002**, *65*, 51505.

(33) Bellour, M.; Skouri, M.; Munch, J. P.; Hebraud, P. Brownian motion of particles embedded in a solution of giant micelles. *Eur. Phys. J. E* **2002**, *8*, 431.

(34) Scheffold, F.; Skipetrov, S. E.; Romer, S.; Schurtenberger, P. Diffusing-wave spectroscopy of nonergodic media. *Phys. Rev. E* **2001**, *63*, 061404.

(35) Zakharov, P.; Cardinaux, F.; Scheffold, F. Multi-speckle diffusing wave spectroscopy with a single mode detection scheme. *Phys. Rev. E* **2006**, *73*, 011413.

(36) Viasnoff, V.; Jurine, S.; Lequeux, F. How are colloidal suspensions that age rejuvenated by strain application? *Faraday Discuss.* **2003**, *123*, 253.

(37) Viasnoff, V.; Lequeux, F.; Pine, D. J. Rev. Multispeckle diffusing-wave spectroscopy: A tool to study slow relaxation and time-dependent dynamics. *Sci. Instrum.* **2002**, *73*, 2336.

(38) Santamaría-Holek, I.; Rubí, J. M.; Gadomski, A. Thermokinetic approach of single particles and clusters involving anomalous diffusion under viscoelastic response. *J. Phys. Chem. B* **2007**, *111*, 2293.
(39) S. de Groot, Mansur, P. *Non-equilibrium Thermodynamics*; Dover: New York, 1984.
(40) Santamaría-Holek, I. Anomalous diffusion in microrheology. *AIP Conference Proceedings of the 5th International Workshop on Complex Systems* **2008**, *982*, 672.
(41) Santamaría-Holek, I.; Rubí, J. M. Finite-size effects in microrheology. *J. Chem. Phys.* **2006**, *125*, 064907.
(42) Doi, M.; Edwards, S. F. *The Theory of Polymer Dynamics*; Claredon: Oxford, U.K., 1986.
(43) Galvan-Miyoshi, J.; Delgado, J.; Castillo, R. Diffusing wave spectroscopy in Maxwellian fluids. *Eur. Phys. J. E* **2008**, *26*, 369.
(44) Ochab-Marcinek, A.; Holyst, R. Scale-dependent diffusion of spheres in solutions of flexible and rigidpolymers: mean square displacement and autocorrelation function for FCS and DLS measurements. *Soft Matter* **2011**, *7*, 7366.
(45) Sarmiento-Gomez, E.; Lopez-Diaz, D.; Castillo, R. Microrheology and Characteristic Lengths in Wormlike Micelles Made of a Zwitterionic Surfactant and SDS in Brine. *J. Phys. Chem. B* **2010**, *114*, 12193.
(46) Sarmiento-Gomez, E.; Montalvan-Sorrosa, D.; Garza, C.; Mas-Oliva, J.; Castillo, R. Rheology and DWS microrheology of concentrated suspensions of the semiflexible filamentous fd virus. *Eur. Phys. J. E* **2012**, *35*, 35.
(47) Tassieri, M.; Evans, R. M. L.; Barbu-Tudoran, L.; Nasir Khaname, F.; Trinick, J.; Waigh, T. A. Dynamics of semiflexible polymer solutions in the highly entangled regime. *Phys. Rev. Lett.* **2008**, *101*, 198301.
(48) D. Ben-Avraham, Havlin, S. *Diffusion and Reactions in Fractals and Disordered Systems*; University Press: Cambridge, U.K., 2000.
(49) Lu, Q.; Solomon, M. J. Probe size effects on the microrheology of associating polymer solutions. *Phys. Rev. E* **2002**, *66*, 061504.
(50) van Zanten, J. H.; Amin, S.; Abdala, A. A. Brownian motion of colloidal spheres in aqueous PEO solutions. *Macromolecules* **2004**, *37*, 3874.
(51) Sarmiento-Gomez, E.; Lopez-Diaz, D.; Castillo, R. Microrheology and Characteristic Lengths in Wormlike Micelles made of a Zwitterionic Surfactant and SDS in Brine. *J. Phys. Chem. B* **2010**, *114*, 12193.